



Article

A Three-Dimensional Conceptual Model for Estimating the Above-Ground Biomass of Winter Wheat Using Digital and Multispectral Unmanned Aerial Vehicle Images at Various Growth Stages

Yongji Zhu ^{1,†}, Jikai Liu ^{1,†}, Xinyu Tao ^{1,†}, Xiangxiang Su ¹, Wenyang Li ², Hainie Zha ^{3,4}, Wenge Wu ^{1,5,*} and Xinwei Li ^{1,6,7,*}

¹ College of Resources and Environment, Anhui Science and Technology University, Chuzhou 233100, China

² College of Agriculture, Anhui Science and Technology University, Chuzhou 233100, China

³ School of Computer and Information, Anqing Normal University, Anqing 246133, China

⁴ Anhui Yigang Information Technology Co., Ltd., Anqing 246003, China

⁵ Rice Research Institute, Anhui Academy of Agricultural Sciences, Hefei 230001, China

⁶ Agricultural Waste Fertilizer Utilization and Cultivated Land Quality Improvement Engineering Research Center, Chuzhou 233100, China

⁷ Anhui Engineering Research Center of Smart Crop Planting and Processing Technology, Chuzhou 233100, China

* Correspondence: wuwenge@vip.sina.com (W.W.); lixw@ahstu.edu.cn (X.L.)

† These authors contributed equally to this work.

Abstract: The timely and accurate estimation of above-ground biomass (AGB) is crucial for indicating crop growth status, assisting management decisions, and predicting grain yield. Unmanned aerial vehicle (UAV) remote sensing technology is a promising approach for monitoring crop biomass. However, the determination of winter wheat AGB based on canopy reflectance is affected by spectral saturation effects. Thus, constructing a generic model for accurately estimating winter wheat AGB using UAV data is significant. In this study, a three-dimensional conceptual model (3DCM) for estimating winter wheat AGB was constructed using plant height (PH) and fractional vegetation cover (FVC). Compared with both the traditional vegetation index model and the traditional multi-feature combination model, the 3DCM yielded the best accuracy for the jointing stage (based on RGB data: coefficient of determination (R^2) = 0.82, normalized root mean square error (nRMSE) = 0.2; based on multispectral (MS) data: R^2 = 0.84, nRMSE = 0.16), but the accuracy decreased significantly when the spike organ appeared. Therefore, the spike number (SN) was added to create a new three-dimensional conceptual model (n3DCM). Under different growth stages and UAV platforms, the n3DCM (RGB: R^2 = 0.73–0.85, nRMSE = 0.17–0.23; MS: R^2 = 0.77–0.84, nRMSE = 0.17–0.23) remarkably outperformed the traditional multi-feature combination model (RGB: R^2 = 0.67–0.88, nRMSE = 0.15–0.25; MS: R^2 = 0.60–0.77, nRMSE = 0.19–0.26) for the estimation accuracy of the AGB. This study suggests that the n3DCM has great potential in resolving spectral errors and monitoring growth parameters, which could be extended to other crops and regions for AGB estimation and field-based high-throughput phenotyping.

Keywords: AGB; UAV; winter wheat; spectral features; three-dimensional conceptual model



Citation: Zhu, Y.; Liu, J.; Tao, X.; Su, X.; Li, W.; Zha, H.; Wu, W.; Li, X. A Three-Dimensional Conceptual Model for Estimating the Above-Ground Biomass of Winter Wheat Using Digital and Multispectral Unmanned Aerial Vehicle Images at Various Growth Stages. *Remote Sens.* **2023**, *15*, 3332. <https://doi.org/10.3390/rs15133332>

Academic Editor: Mario Cunha

Received: 15 May 2023

Revised: 25 June 2023

Accepted: 27 June 2023

Published: 29 June 2023



Copyright: © 2023 by the authors. Licensee MDPI, Basel, Switzerland. This article is an open access article distributed under the terms and conditions of the Creative Commons Attribution (CC BY) license (<https://creativecommons.org/licenses/by/4.0/>).

1. Introduction

Winter wheat is one of the world's major cereal crops, accounting for 18% of the cultivated area in China [1]. Its yield is also crucial for international grain trade and global food security [2–4]. The AGB is a critical indicator in crop growth status assessment, farm management, and grain yield prediction [5,6]. Traditional measurements of AGB in the laboratory are destructive and time-consuming; the measurements are highly accurate

but challenging to promote on a large scale [7,8]. Therefore, the timely, efficient, and accurate monitoring of winter wheat AGB is important for effective field management and increasing yield [9,10].

Compared with traditional measurement methods, remote sensing as a non-destructive technique has been demonstrated to have great potential in the measurement of AGB due to its simplicity and efficiency [11–13]. Various remote sensing platforms can capture crop canopy reflection spectrum signals to monitor crop biophysical/biochemical parameters [14,15]. These platforms that have been used to monitor crop AGB include near-surface hyperspectral systems [16,17], unmanned aerial vehicles (UAVs) [18–20], and satellites [21–23]. Although near-surface hyperspectral systems and satellite images have high spectral resolution and a wide field of view [24,25], UAV platforms have great potential in crop phenotype monitoring due to their low cost and simple operation [26,27]. Most studies of AGB have been conducted using vegetation indices (VIs), e.g., the normalized difference vegetation index (NDVI [28]) and excess green (ExG [29]), which have achieved remarkable research results [30–33]. However, some studies have shown that the spectral saturation effect significantly impacts the estimation of crop biochemical parameters [34–37]. In particular, VIs constructed using the red and near-infrared bands can easily result in spectral saturation under conditions of high crop coverage [35,38,39]. Especially for upright-growing crops, such as winter wheat and corn, dense and compact planting modes will inevitably produce dense canopy growth. Another issue is that VIs are insensitive to AGB during the reproductive growth stage, which is because the reflection and absorption of light of different wavelengths by the chlorophyll in the canopy are saturated at this stage [38,40]. The spectral features have nonlinear relationships with physiological and biochemical parameters, and the sensitivity of these features to crop biochemical parameters is low during the reproductive growth stage [41,42]. These factors limit the ability of VIs to estimate crop physiological and biochemical parameters at different growth stages.

Several researchers have made efforts to address the saturation problem in crop estimation, such as improving or constructing vegetation indices [39,43,44] or integrating texture features [38,45], structural features [46–48], and fractional vegetation cover (FVC) [49,50] into estimation models. Generally, the combination of multi-source features can provide higher accuracy in AGB estimation and reduce the influence of the spectral saturation effect on the model [47,51,52]. However, many studies have tended to use multiple features as independent model input factors to estimate target features, leading to the accuracy of traditional multi-feature combination models being unstable under different research and experimental conditions [53]. Therefore, to ensure the stability and universality of models, a more efficient method of feature combination must be found. For example, considering that maize AGB is composed of stems and leaves before the tasseling stage, Shu et al. [54] constructed a three-dimensional conceptual model (3DCM) for predicting maize AGB by integrating the leaf area index (LAI) and plant height (PH) to improve the accuracy of using UAV data to monitor the maize AGB at the jointing stage. However, it is still unclear whether the 3DCM can be applied to estimate the AGB of winter wheat, whether it is suitable for different growth stages, and whether the 3DCM has better accuracy than the traditional multi-feature combination model. Therefore, it is necessary to explore the potential of the 3DCM for winter wheat AGB estimation.

Recent studies have reported high-dimensional data and non-linear relationships, posing new challenges to current data processing methods [55]. Compared with traditional regression techniques, machine learning (ML) algorithms are typically better at handling high-dimensional data and non-linear relationships between the predictor variable and target variable [56–58]. Currently, ML regression algorithms such as the support vector machine (SVM) [59,60], artificial neural network (ANN) [61,62], and random forest (RF) [63,64] have been widely used to integrate multi-source input variables, including integrating VIs and plant height [48], integrating VIs and thermal characteristics [65], and integrating texture, color, and VIs [66]. However, the winter wheat AGB prediction improvement through traditional multi-source feature combinations is limited. Therefore, it is necessary to consider the

contributions of characteristic variables to the estimation of AGB and accurately estimate winter wheat AGB by effectively combining the characteristic variables.

Therefore, this research aimed to establish a 3DCM for the accurate estimation of winter wheat AGB across multiple stages. The specific objectives of this study were as follows: (1) to construct a new three-dimensional conceptual model (n3DCM), (2) to evaluate the potential of the n3DCM in AGB estimation, and (3) to compare the advantages of different UAVs in AGB estimation.

2. Materials and Methods

2.1. Experimental Design

The winter wheat field experiment was conducted in the 2021 growing season. The winter wheat experiment site was located at Xiaogang Village, Fengyang County, Chuzhou City, Anhui Province in China (117°42'E, 32°16'N) (Figure 1).

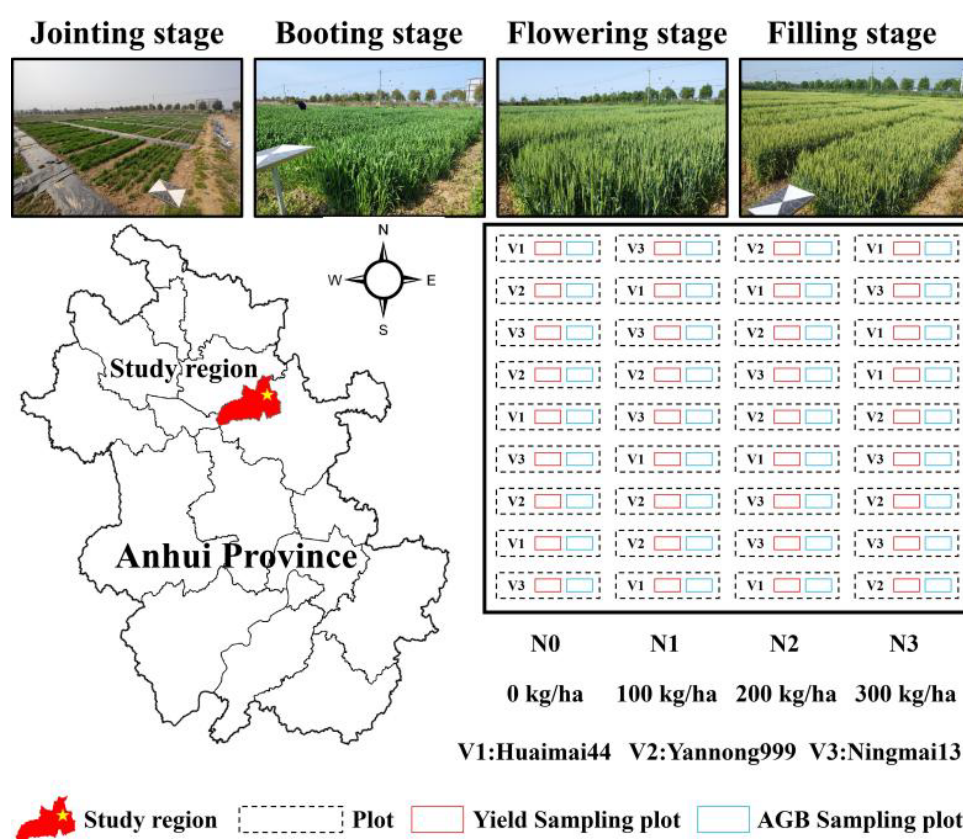


Figure 1. Location of the experimental site and the experimental design of the winter wheat field plots in 2021.

Different winter wheat cultivars and nitrogen (N) fertilizer treatments were set up in the experiment. The plot number was 36 and the plot size was 2 m × 8 m. The three winter wheat cultivars were Huaimai 44 (V1, high-gluten wheat), Yannong 999 (V2, high-gluten wheat), and Ningmai 13 (V3, low-gluten wheat), with three replicates of each. The four nitrogen fertilizer treatments were N0 (0 kg/ha), N1 (100 kg/ha), N2 (200 kg/ha), and N3 (300 kg/ha). The N fertilizer was applied in the form of urea, with 60% applied before planting and 40% applied during the jointing stage. Other management practices were consistent with local recommendations.

2.2. Field Data Collection

In 2021, 36 plots were sampled to measure the PH and winter wheat AGB at four critical growth stages. Three winter wheat plants from a sample plot were randomly

selected, and their distances from the highest point to the ground were measured using a ruler. The average value was then taken as the true plant height in the sample plot.

The winter wheat AGB was measured via manually destructive sampling from two rows. Each sample was 0.5 m long. These winter wheat samples were quickly transported to the lab for leaf, stem, and spike separation. All fresh organs were oven-dried at 105 °C for 30 min and then at 75 °C for at least 24 h to achieve a constant weight. The dry weight of the winter wheat was then obtained using a balance (accuracy: 0.01 g) and the AGB was then converted to kg/ha.

At the mature stage of winter wheat, 1 m² of wheat with consistent growth was randomly selected from each plot in the study area. The yield and SN of winter wheat samples were obtained after threshing, drying to constant weight, and weighing.

2.3. Data Acquisition

2.3.1. Acquisition of the UAV Images

This study employed a DJI Mavic 2 (DJI Technology Co., Shenzhen, China) with an RGB digital camera to acquire high spatial-resolution image and a DJI Phantom 4 multispectral (DJI Technology Co., Shenzhen, China) to capture the multispectral image. The UAV images of winter wheat were acquired before sowing and at critical growth stages (jointing, booting, flowering, and filling). The DJI GS pro software package (<https://www.dji.com/cn/downloads/djiapp/dji-gs-pro>, accessed on 13 May 2023) was used to design the same flight plans for all campaigns. The flight altitude was set to 30 m (pixel size: 0.7 cm for RGB data, 1.5 cm for multispectral (MS) data) with a flight speed of 2 m/s. The forward overlap of images was higher than 90% and the side overlap was higher than 85%. Four standard reflector panels were placed on the ground for radiometric calibration, and five ground control points were evenly distributed in the field. All UAV flights were conducted from 10 a.m. to 2 p.m. on sunny and cloudless days. The UAV camera specifications and data acquisition dates are shown in Table 1.

Table 1. Camera specifications and summary of field campaigns for the wheat experiments.

Camera	Spectral Band (nm)	Date of UAV Flight	Growth Stage
RGB	Red	14 March 2021	Jointing
	Green		
	Blue		
MS	Blue (450 ± 16 nm)	8 April 2021	Booting
	Green (560 ± 16 nm)	29 April 2021	Flowering
	Red (650 ± 16 nm)	9 May 2021	Filling
	Red edge (730 ± 16 nm)		
	Near-infrared (840 ± 26 nm)		

2.3.2. Preprocessing of the UAV Images

The RGB and MS image mosaicking was conducted with the PIX4Dmapper software (4.4.12 version, Pix4D SA, Prilly, Switzerland) to generate ortho-mosaics from four critical growth stages. The main operations of this procedure mainly include aligning the images, adding ground control points, generating dense point clouds and texture meshes, reconstructing 3D images based on structure from a motion (SfM) algorithm [67], and, finally, obtaining the digital orthophoto model (DOM), digital surface model (DSM), and digital terrain model (DTM) images of the study area. The images of reflector panels on the ground were collected for radiometric calibration. ArcGIS (10.2 version, Environmental Systems Research Institute, Inc., Redlands, CA, USA) was used to create all plots' vector boundaries. To minimize the impact of marginal effects, the edge of each plot was omitted while creating the .shp file. The average of all the extracted pixel values of each plot was used as the corresponding feature.

2.4. Methods

The PH and FVC values extracted from the UAV data were used to construct a 3DCM for estimating the AGB of winter wheat. The critical process is shown in Figure 2. First, the canopy height model (CHM) was used to obtain the PH of winter wheat. Second, the VI was extracted from UAV images, and the FVC of each plot was extracted using the “excess green (ExG)—excess red (ExR)” method. Third, different models were trained and verified. Fourth, the accuracy of different models was compared and the AGB was visualized.

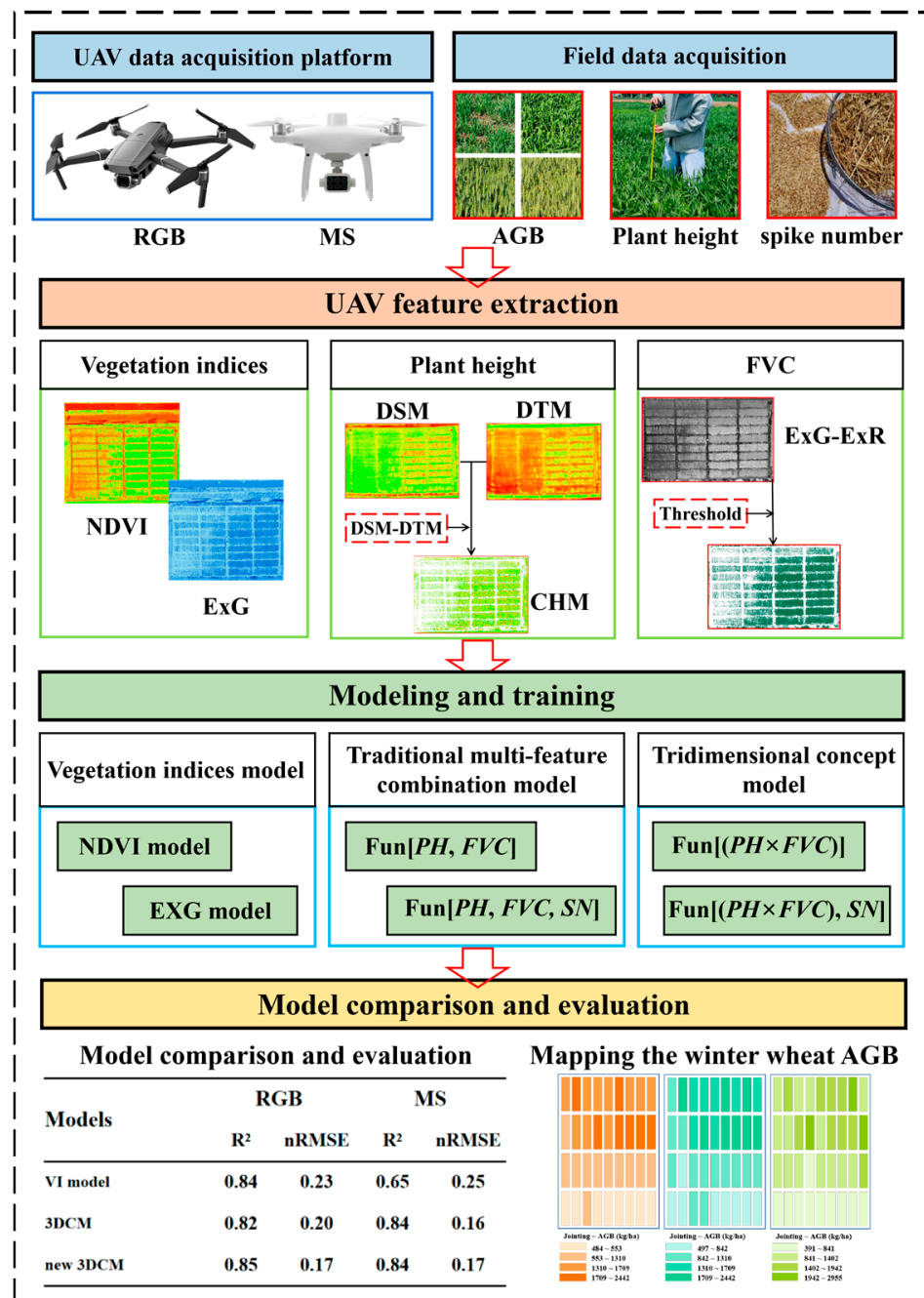


Figure 2. Research flow map.

2.4.1. PH Extraction

Before planting the winter wheat, we used UAVs to obtain the terrain model of the fields. Then, we used the UAVs to acquire the winter wheat’s DSM at different growth

stages and subtracted the DTM from the DSM at each growth stage to extract the plant height of the winter wheat. The calculation method is shown as Equation (1):

$$CHM = DSM_i - DTM_0, \quad (1)$$

where DSM_i represents the DSM generated in the i th stage and DTM_0 represents the terrain DTM obtained before planting. As shown in Figure 3, the measured and extracted PHs exhibited good consistency (RGB: $R^2 = 0.76$; MS: $R^2 = 0.88$). Overall, the extracted PH was slightly lower compared to the measured PH.

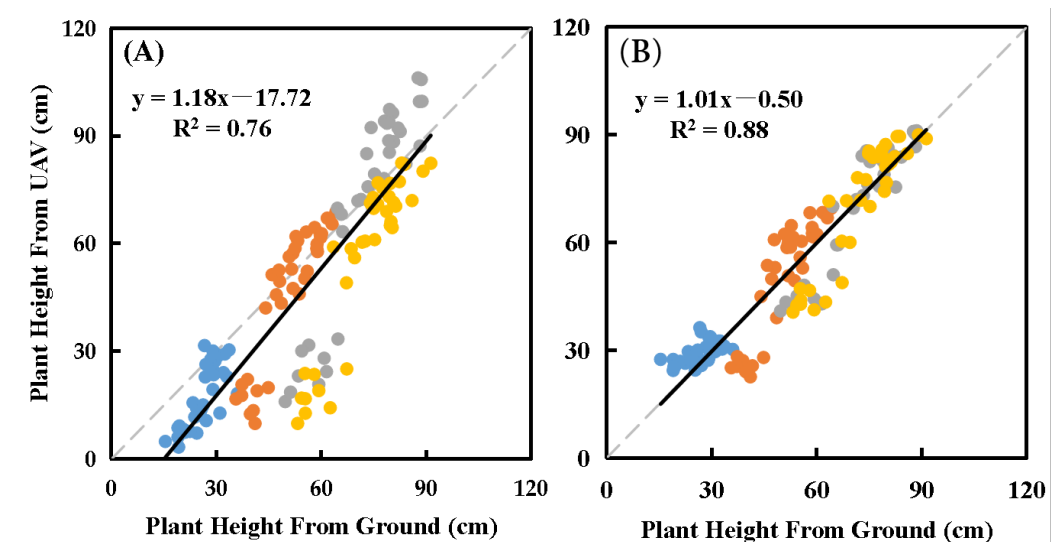


Figure 3. Comparison between the measured plant height and the plant height derived from unmanned aerial vehicle (UAV) images ((A): RGB; (B): MS).

2.4.2. FVC Calculation

FVC is usually defined as the percentage of the vertical projection area of vegetation (including branches, stems, and leaves) in a unit area [68]. In this study, the “ExG–ExR” method was used to segment soil background pixels from original images, which is effective for different soil backgrounds and has excellent performance in processing natural color digital images [69]. The FVC of each plot was calculated using Equation (2):

$$FVC = \frac{N_{\text{green}}}{N_{\text{all}}}, \quad (2)$$

where N_{all} represents the full number of pixels in one plot and N_{green} represents the number of pixels after removing the background.

2.4.3. Machine Learning Algorithm

RF, which was proposed by Breiman [70], is commonly used in the estimation of the AGB of winter wheat [71,72]. The RF model combines a large number of trees to improve accuracy [73]. RF regression not only handles a large number of input variables but also uses small subsets of variables to obtain a reasonable prediction accuracy. In addition, RF regression can help overcome the overfitting issue of simple decision trees [31,74]. There are three parameters, including the number of trees (ntree), the number of variables used as predictors for each tree (mtry), and the minimum size for each terminal mode (node size) [75]. This paper set ntree to 1000 and mtry to 1 to 2.

2.4.4. Three-Dimensional Conceptual Model

Many studies have shown a good correlation between PH and AGB [7,30,33,76]. Most studies combine the PH value with spectral and texture characteristics to estimate winter wheat biomass, but the accuracy of this method varies across different studies. Therefore,

to estimate winter wheat AGB accurately and stably, this study established a 3DCM for estimating the AGB based on the work of Shu et al. [54] (Figure 4B). Before the heading stage, the winter wheat AGB was composed of stems and leaves. Different winter wheat varieties have different stem heights. The stem height is associated with stem weight [77]. The number and area of leaves determine the weight of the leaves. FVC refers to the percentage of the vertical projection area of the canopy to the total area and is highly correlated with the leaf biomass. Although the VI was the same, the biomass varied with stem height. Therefore, it was necessary to consider differences in PH to improve the accuracy of the AGB estimates. A winter wheat population can be regarded as a cube. The FVC is the base area of the winter wheat cube. The larger the FVC value, the larger the bottom area of the cube. The height of the cube is represented in the PH value. The higher the PH, the higher the height of the winter wheat cube. The volume of the cube is calculated by multiplying the area of its base by its height. Therefore, before the heading stage of winter wheat, AGB could be estimated using Equation (3).

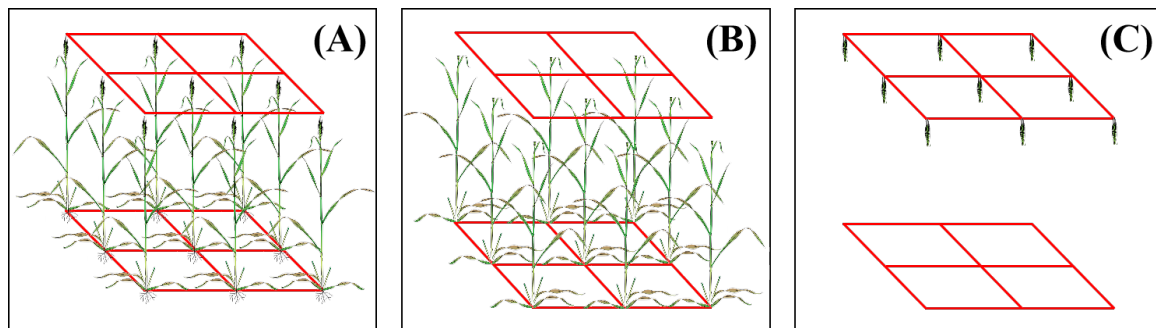


Figure 4. Conceptual map of the prediction model for above-ground biomass of winter wheat based on plant height, spike number, and fractional vegetation cover ((A) winter wheat population after the jointing stage; (B) winter wheat population at the jointing stage; (C) spike organs of winter wheat population).

However, Shu et al. [54] only focused on the jointing stage (no spike organ appeared). Therefore, to enhance the stability and universality of the model during the entire growth cycle, attention needed to be paid to the influence of spike organ emergence. Therefore, the present study used the SN to quantify the contribution of spike organs to the AGB (Figure 4A,C). A larger SN value indicated that there were more spike organs and that the AGB of spike organs was larger in the winter wheat population. The influence of spike organs on the AGB of winter wheat was represented by the SN, and the n3DCM was proposed to improve the accuracy of AGB estimation (Equation (4)):

$$M1 : AGB = Fun[(PH \times FVC)] \quad (3)$$

$$M2 : AGB = Fun[(PH \times FVC), SN] \quad (4)$$

where *PH* is the plant height, *SN* is the number of spikes, and *FVC* represents the fractional vegetation cover. *Fun* represents the RF algorithm.

2.5. Accuracy Evaluation

The study dataset was divided into two portions, with 70% of the samples used for calibration and 30% used for validation. This resulted in 25 calibration samples and 11 validation samples. Two metrics of the coefficient of determination (R^2) and normalized root mean square error (nRMSE) were used to evaluate the accuracy of the calibration and validation models as follows:

$$R^2 = 1 - \frac{\sum_{i=1}^n (y_i - x_i)^2}{\sum_{i=1}^n (x_i - \bar{x})^2} \tag{5}$$

$$nRMSE = \frac{\sqrt{\frac{1}{n} \sum_{i=1}^n (y_i - x_i)^2}}{\bar{x}} \tag{6}$$

where x_i and y_i represent the measured and predicted winter wheat AGB for sample i , respectively; \bar{x} is the average measured winter wheat AGB and n is the number of samples.

3. Results

3.1. Comparison of the Ability to Estimate the AGB of Winter Wheat between the Three-Dimensional Conceptual Model (3DCM) and the Traditional VI Model of Different Growth Stages

The R^2 and nRMSE for the AGB simulated using the VI model and the 3DCM are displayed in Figure 5. In general, the two models exhibited greater estimation accuracy values in the jointing stage than in other growth stages. In addition, the RGB or MS accuracy values for the 3DCM (jointing: RGB: $R^2 = 0.82$, nRMSE = 0.20; MS: $R^2 = 0.84$, nRMSE = 0.16) were higher than those for the VI model. Among them, compared with the 3DCM, the R^2 was slightly higher for the VI model RGB-based ExG at the jointing stage, but the nRMSE of AGB estimated using the VI model was larger. The results demonstrated that the 3DCM could yield satisfactory accuracy in the jointing stage, which is similar to the finding of Shu et al. [54].

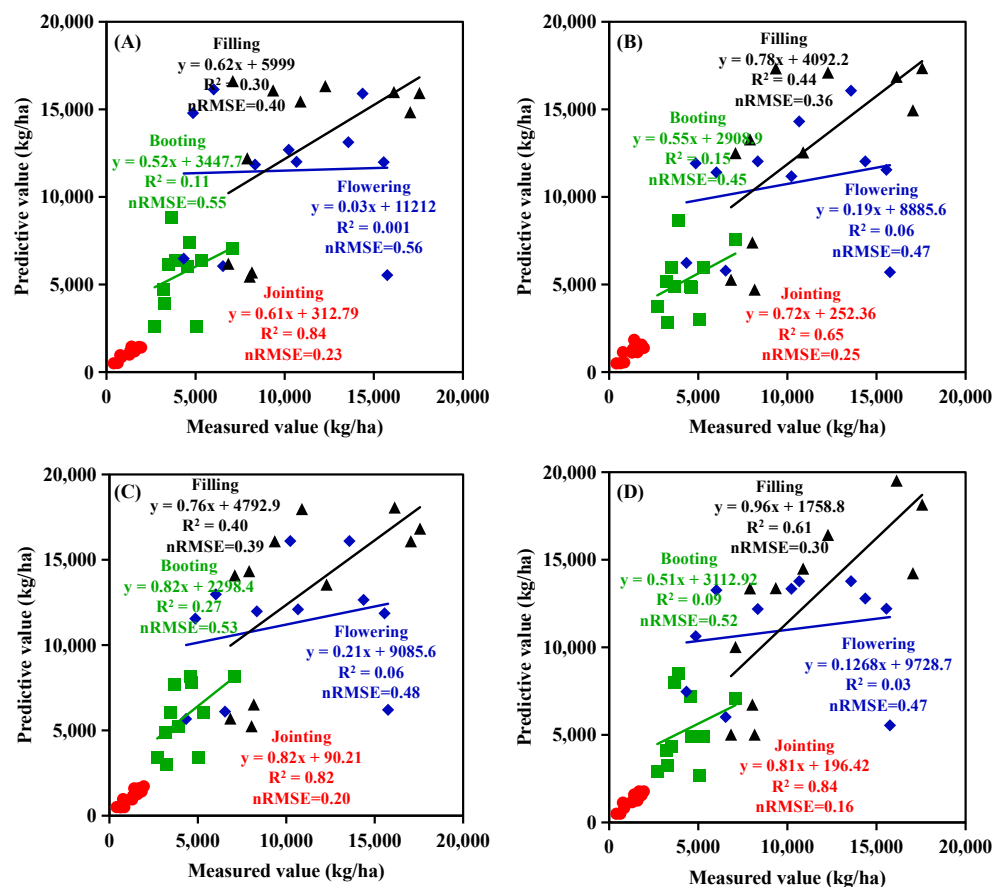


Figure 5. Relationship between measured and predicted above-ground biomass (AGB) based on the traditional vegetation model. ((A,B) Traditional vegetation model; (C,D) 3DCM; (A,C) RGB; (B,D) multispectral). Coefficient of determination, R^2 ; normalized root mean square error, nRMSE.

3.2. Differences between the Three-Dimensional Conceptual Model (3DCM) and the Traditional Multi-Feature Combination Model in Estimating Winter Wheat AGB

Figure 6 shows a comparison of the 3DCM and traditional multi-feature combination model for the estimation of AGB across the critical growth stages. Compared with the 3DCM, the performance of the traditional multi-feature combination model was lower than that of the 3DCM in the jointing stage. In addition, the traditional multi-feature combination model also showed a similar decrease in accuracy after the jointing stage. In the jointing stage, the traditional multi-feature combination model achieved the best accuracy (RGB: $R^2 = 0.76$, $nRMSE = 0.21$; MS: $R^2 = 0.70$, $nRMSE = 0.21$) among the four growth stages. At the stages of the emergence of spike organs, the accuracy of the traditional multi-feature combination model was higher than that of the 3DCM, indicating that the 3DCM had high consistency with the winter wheat AGB at the jointing stage without the appearance of the spike organ. However, after the formation of the spike organ, the 3DCM needed more description of spike characteristics, which resulted in the poor performance of estimating the winter wheat AGB.

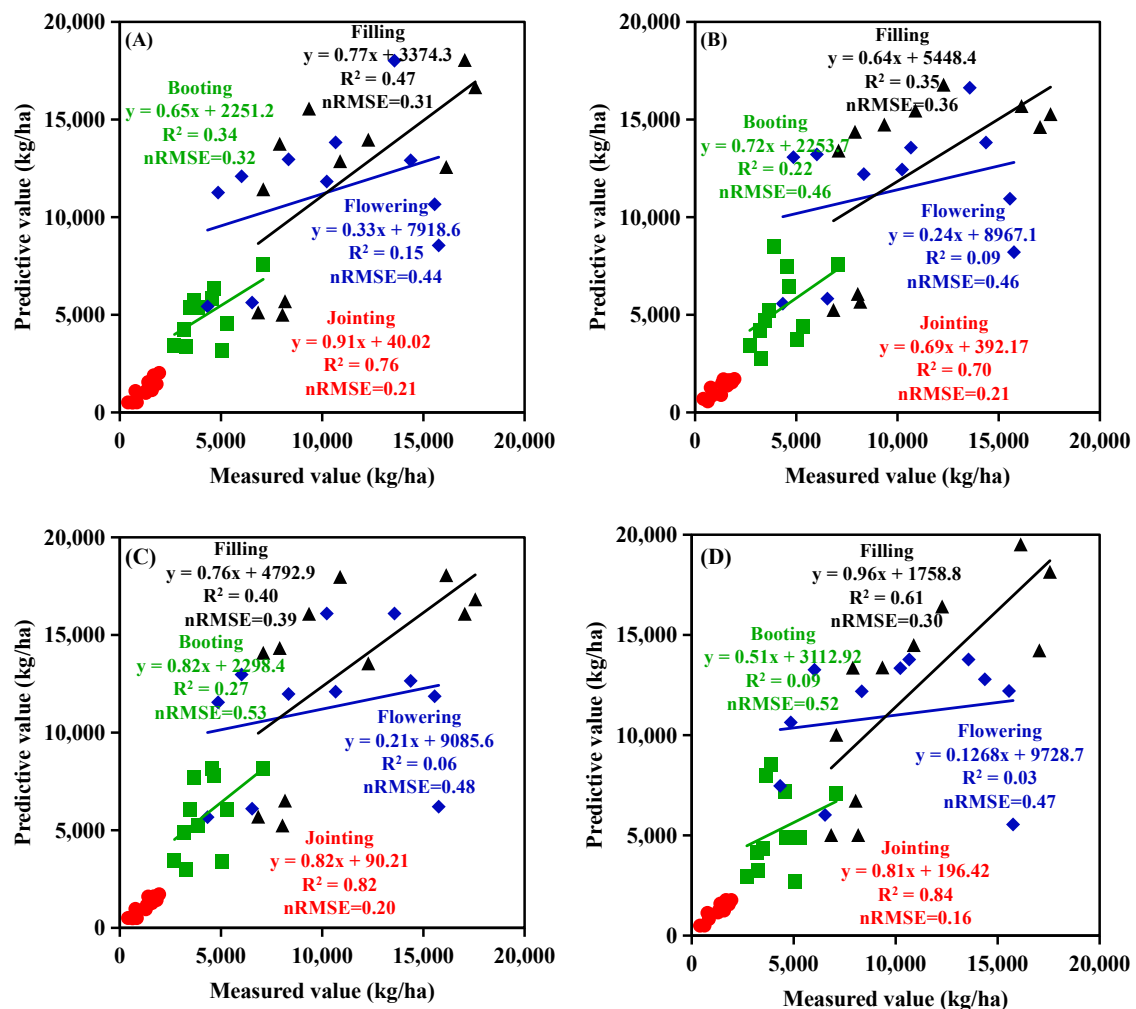


Figure 6. Traditional multi-feature combination model and 3DCM was used to estimate winter wheat above-ground biomass (AGB) at different growth stages based on RGB and multispectral (MS) UAV. ((A,B) Traditional multi-feature combination model; (C,D) 3DCM; (A,C) RGB; (B,D) MS). Coefficient of determination, R^2 ; normalized root mean square error, $nRMSE$.

3.3. The Three-Dimensional Conceptual Model (3DCM) with Spike Organ Consideration

To improve the accuracy of the 3DCM in estimating winter wheat AGB and broaden the usability of the model at different growth stages, this study introduced a feature highly

correlated with spike weight: the SN. The SN and $PH \times FVC$ were used as input factors to construct an n3DCM. To explore the performance of the n3DCM in estimating the winter wheat AGB under different UAVs and growth stages, this study compared its performance with that of the n3DCM and the traditional multi-feature combination model (PH, FVC, and SN). The results are shown in Figure 7.

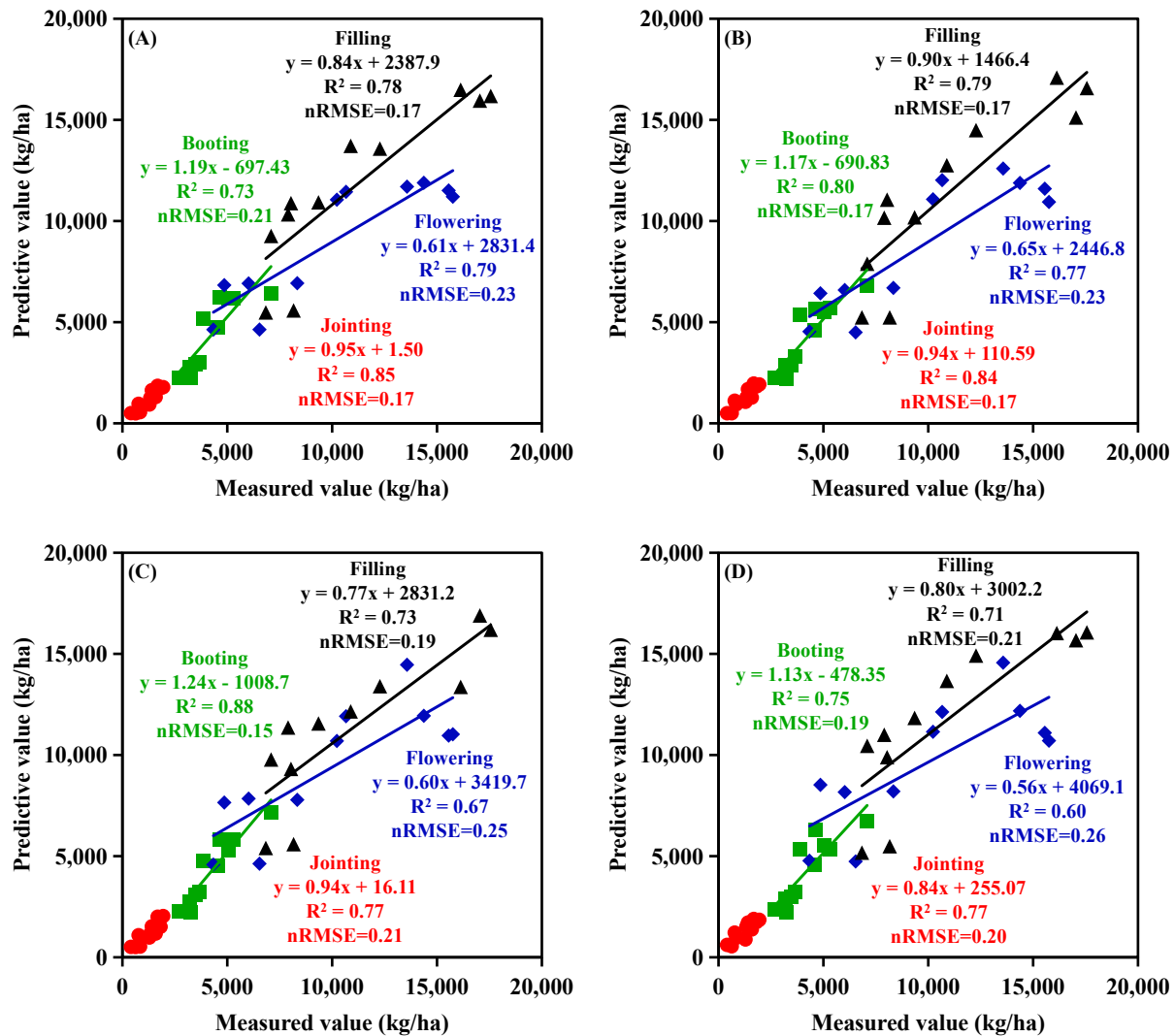


Figure 7. Traditional multi-feature combination model and n3DCM was used to estimate winter wheat above-ground biomass (AGB) at different growth stages based on RGB and multispectral (MS) UAV. ((A,B) n3DCM; (C,D) traditional multi-feature combination model; (A,C) RGB; (B,D) MS). Coefficient of determination, R^2 ; normalized root mean square error, nRMSE.

The results of winter wheat AGB estimation using the n3DCM are shown in Figure 7A,B). The accuracy of the n3DCM was significantly better than that of the 3DCM (Figure 6C,D). The R^2 and nRMSE of winter wheat AGB were estimated to be above 0.73 and below 0.21, respectively, using the n3DCM based on different UAV and growth stages. Compared with the 3DCM, the accuracy of the n3DCM was not significantly improved at the jointing stage, but it was significantly improved after the jointing stage. Compared with the 3DCM (Figure 6C,D), the accuracy of the n3DCM improved most significantly in estimating the AGB of winter wheat during the flowering stage; the R^2 increased from 0.06 to 0.79 and the nRMSE decreased from 0.48 to 0.23 for the RGB UAV. Under the MS UAV, the R^2 increased from 0.03 to 0.77 and the nRMSE decreased from 0.47 to 0.23. Furthermore, the n3DCM

exhibits high and consistent accuracy in estimating winter wheat AGB across different UAVs and growth stages.

Based on the traditional multi-feature combination model, the FVC, PH, and SN were used as input features of the model to estimate the winter wheat AGB. The results are shown in Figure 7C,D. Overall, the accuracy of the n3DCM was higher than that of the traditional multi-feature combination model. However, the accuracy of the traditional multi-feature combination model was better than that of the n3DCM when predicting the winter wheat AGB based on RGB UAV data at the booting stage, and the R^2 and nRMSE were 0.88 and 0.15 for the traditional multi-feature combination model, respectively, and 0.73 and 0.21 for the n3DCM, respectively. The changing pattern of the traditional multi-feature combination model based on the FVC, PH, and SN was similar to that of the traditional multi-feature combination model based on the FVC and PH. Adding the SN feature significantly improved the accuracy of AGB estimation at the booting, flowering, and filling stages. However, there was no apparent improvement at the jointing stage. The 3DCM also showed the same difference. These results indicate that the SN feature has great potential in estimating the AGB during spike organ emergence. In general, the n3DCM with the SN feature had the best performance in AGB estimation, and the model had stable performance in different growth stages and with different UAVs. These results indicate that n3DCM is better than the traditional multi-feature combination model and 3DCM.

3.4. The Performance of Multi-Sensor Fusion in AGB Estimation

The PH and FVC features extracted from RGB and MS images were fused for estimating the winter wheat AGB. The results are shown in Figure 8. The accuracy of the n3DCM combining the PH and FVC extracted from different UAVs was lower than that based on a single UAV. The n3DCM that combined PH values based on MS and the FVC value based on RGB had the lowest accuracy for the jointing stage ($R^2 = 0.58$, nRMSE = 0.26). Overall, these results indicated that mixed multi-source UAV features did not necessarily improve the AGB estimation accuracy.

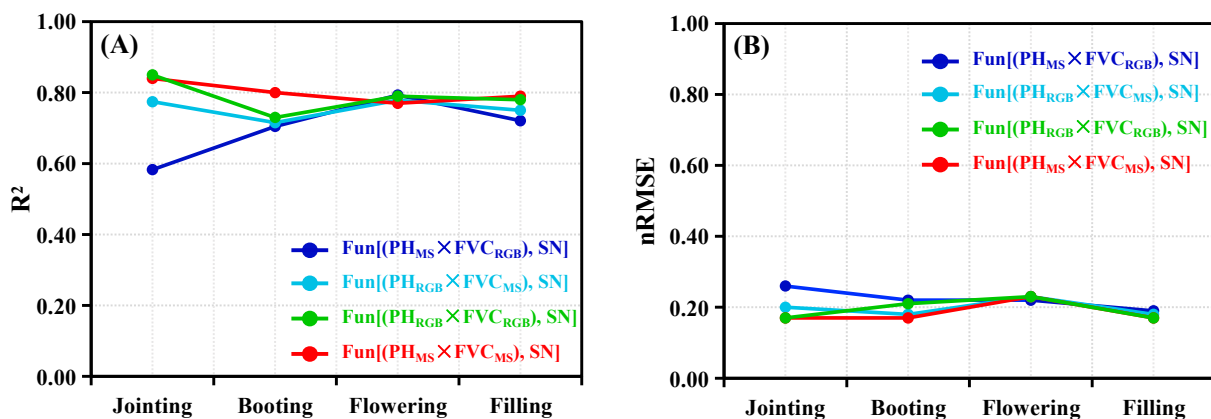


Figure 8. Results of winter wheat above-ground biomass (AGB) estimation using a new three-dimensional conceptual model integrating multi-source unmanned aerial vehicle (UAV) features. ((A) The determination coefficients of winter wheat AGB monitoring with UAV features and single UAV features; (B) nRMSE for monitoring winter wheat AGB with UAV feature fusion and single UAV features). Coefficient of determination, R^2 ; normalized root mean square error, nRMSE.

3.5. AGB Mapping Using the New Three-Dimensional Conceptual Model (n3DCM)

We mapped the winter wheat AGB using n3DCM and two types of UAV data (Figure 9). The n3DCM based on MS had higher accuracy in estimating AGB. The n3DCM based on RGB showed clear underestimation in the N0 region during the jointing stage. In booting images, there was an overestimation in the N0 region and an underestimation in the N3 region.

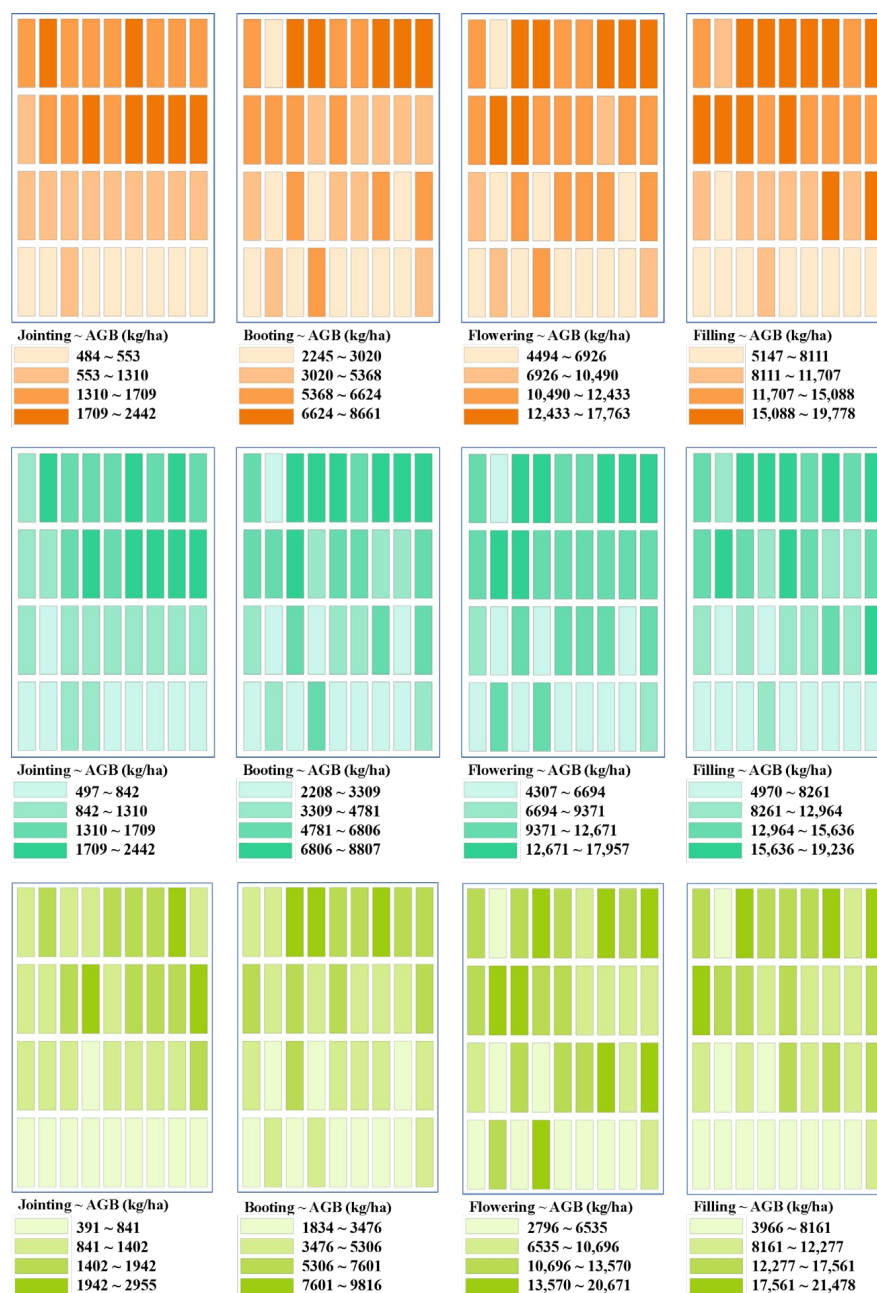


Figure 9. The map of estimated winter wheat AGB using the new three-dimensional conceptual model (first row: RGB; middle row: MS; bottom row: measured value).

4. Discussion

4.1. Limitations of Spectral Information for Monitoring Crops

Remote sensing technology allows for efficient and convenient estimates of crop biophysical/biochemical parameters using canopy spectral reflectance, but the spectral saturation phenomenon can significantly affect the accuracy of the model. Our study also showed that spectral features alone could not reasonably estimate the AGB of winter wheat during the whole growth stage (Figure 5A,B). The variation pattern of NDVI and AGB in Figure 10 shows that with increases in AGB in winter wheat, the VI produced a relatively saturated effect, resulting significant decrease in the ability of VI to estimate AGB.

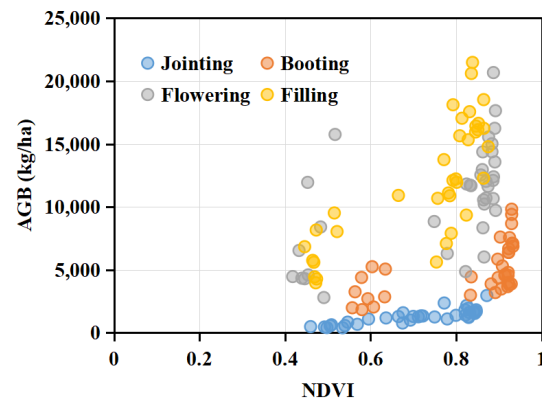


Figure 10. Changes in normalized difference vegetation index (NDVI) and above-ground biomass (AGB).

Over the past few decades, various schemes have been proposed to overcome the effect of spectral saturation on crop AGB estimates. Although the problem of saturation in spectral features has been partially overcome, spectral signals are susceptible to various factors in real situations. In the field scene, soil background, moisture, spectral acquisition time, spatial image resolution, and other factors will affect the spectral signals [16,31,78,79]. As shown in Figure 11, taking jointing stage as an example, the difference in green pixel reflectance and all pixel reflectance was determined under various N fertilizer treatments. With both UAVs, the reflectance increased when the background was removed. The vegetation coverage under the N0 treatment was relatively low, and GreenPix and AllPix differed significantly in red, red-edge, and near-infrared bands. With the increase in coverage, the gap between GreenPix and AllPix in red, red-edge, and near-infrared bands became smaller and gradually tended to be the same, only being slightly different in near-infrared bands. This shows that background has a strong influence on spectral characteristics.

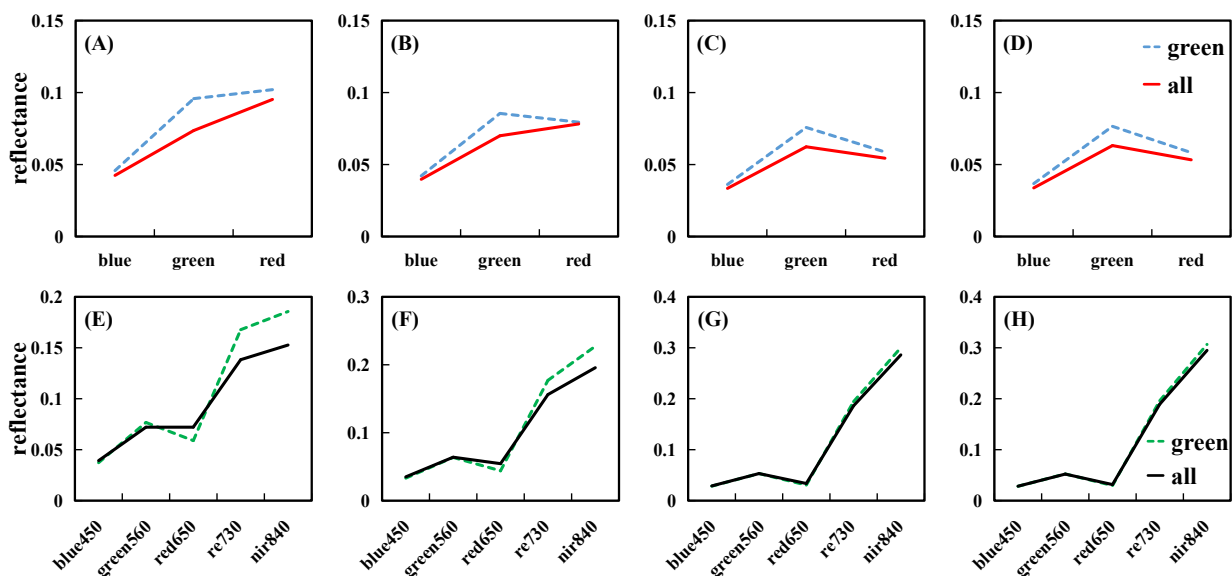


Figure 11. Comparison of the average reflectance of all pixels (all) and wheat pixels (green) under different nitrogen fertilizer treatments ((A–D) RGB; (E–H) (multispectral) MS; (A,E) nitrogen rate: 0 kg/ha; (B,F) nitrogen rate: 100 kg/ha; (C,G) nitrogen rate: 200 kg/ha; (D,H) nitrogen rate: 300 kg/ha). The solid line represents all pixels, while the dashed line represents green pixels.

The spectral signal collected by UAV are generally of the leaf canopy, which correlate well with the biochemical parameters of leaves. However, winter wheat AGB is composed of multiple organs; thus, it is not appropriate to estimate the sum of leaf, stem, and spike organs using only the spectral signal of the canopy [62]. Because the zenith angle makes

it challenging to obtain spectral signals of crop stems or below the canopy, in order to collect more spectral information reflected by crop organs and reduce the contribution of the soil background to the spectral reflectance of the canopy, some studies have obtained multi-angle image data by adjusting the shooting angle of the UAV [80,81]. In addition, several studies have collected spectral reflectance at different times to obtain more spectral signals of the physiological and biochemical parameters of crops by using the changes in the solar altitude angle [19,82]. However, the dense planting pattern of winter wheat prevents the sensor from acquiring spectral signals reflected by all crop organs. Therefore, in a relatively complex field environment, it is necessary to consider using characteristic information that is not affected by natural conditions to estimate the AGB of winter wheat.

4.2. Estimating the AGB Potential of Three-Dimensional Information in Winter Wheat

The canopy reflectance of crops can be affected by the complex interaction between sunlight, vegetation, and soil, and this effect is difficult to eliminate in existing field trials [83]. Because the AGB of winter wheat contains the weight of leaves, stems, and spikes, the dense canopy structure hinders the spectral signal acquisition of stems in the middle and late growing season, and the spectral reflectance cannot reflect the weight of winter wheat stems well.

The PH is an important indicator for characterizing the AGB of the vertical growing crops. Previous studies have shown a moderate correlation between the PH and the crop AGB [46,77,84]. The present study also found a moderate correlation between the PH and the crop AGB (Table 2). Moreover, the CHM-derived PH was slightly lower than the field measurements (Figure 3). Bendig et al. [48] found that there is a degree of underestimation when UAVs are used to estimate plant height. The cause of this underestimation may be that in the field environment, the wind can blow the leaves of winter wheat, resulting in positional changes and differences in the same leaf in the overlapping images captured by the UAV. This leads to the stitched image being unable to accurately reflect the height of the winter wheat. In addition, the maximum spatial resolution of the UAV used in our study was 0.7 cm, which made it difficult to capture the height of the top of the winter wheat canopy for very narrow winter wheat plants. This also leads to the underestimation of plant height.

Table 2. Correlation between the AGB with the FVC, PH, and spike number at different growth stages.

Growth Stage	Fractional Vegetation Cover		Plant Height		Spike Number
	RGB	MS	RGB	MS	
Jointing stage	0.81	0.81	0.75	0.77	0.41
Booting stage	0.28	0.54	0.62	0.63	0.82
Flowering stage	0.37	0.51	0.61	0.67	0.91
Filling stage	0.39	0.71	0.78	0.79	0.82

The FVC is a vital feature in characterizing a canopy and is closely related to the canopy organ and the leaf area index (LAI) [85]. Compared with the LAI, acquiring the FVC is more straightforward and does not require field measurement data. As shown in Table 2, the correlation between the FVC obtained using the two UAVs and the AGB of winter wheat showed the maximum value at the jointing stage, indicating that the FVC at the jointing stage was highly correlated with the AGB of winter wheat. As shown in Figure 12, the AGB at the jointing stage was mainly composed of the leaf organ, which did not show stratification or overlap, and the FVC could well represent the leaf organ. Yue et al. [62] also showed that the leaf organ made up a large proportion in the jointing stage, and leaf features such as the FVC could effectively improve estimation accuracy.

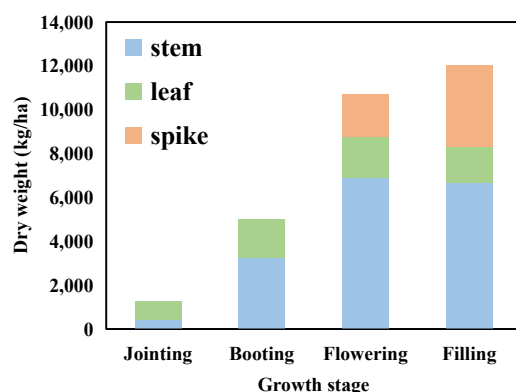


Figure 12. Proportion of different organs (stem, leaf, and spike) in the above-ground biomass at different growth stages.

The PH and FVC used in this study were derived from the CHM and orthophoto images, respectively, which were generated from overlapping images acquired by RGB and MS UAVs. The combination of the PH and FVC as input data for regression techniques is equivalent to using two types of features, namely, vertical and canopy features. The results show that the 3DCM using a combination of PH and FVC information estimated AGB with higher accuracy than models using the VI (Figures 5A,B and 6A,B). However, the accuracy of PH combined with FVC was higher only in the jointing stage, and the model's accuracy in other growth stages could not satisfy the application requirements, indicating that the influence of the spike organ on the model should be considered.

As shown in Figure 12, spike organs appeared after the booting stage, and the weight of spike organs gradually increased with the winter wheat grows, making it necessary to consider the contribution of spike organs to the AGB when estimating the AGB in winter wheat. However, most current studies estimate the AGB using information on spectral, textural, thermal characteristics, PH, and canopy features [10,38,47,54], but the relationship between these characteristics and spike organs is not significant, making it difficult to quantify the weight of spike organs in winter wheat AGB. As shown in Table 2, in the analysis of the correlation between the SN and winter wheat, the SN was better correlated with the winter wheat AGB when spike organs were appearance. Therefore, this study used SN to quantify the contributions of spike characteristics to the winter wheat AGB to enhance the ability of the model to estimate the winter wheat AGB at different growth stages. The PH, FVC, and SN were used as input characteristics to estimate the winter wheat AGB (Figure 7C,D). Adding spike characteristics significantly improved the PH and FVC models after the jointing stage. This indicates that the SN has great potential in estimating winter wheat AGB.

Three-dimensional information has great potential for estimating the AGB in winter wheat, but a simple data feature input may not improve model accuracy [86]. Therefore, the form of the feature combination must be considered to improve the estimation ability of the model.

4.3. Potential Estimation of Winter Wheat AGB Using a New Three-Dimensional Conceptual Model (n3DCM) and the Performance of Multi-Source Data Fusion

Previous studies have found that the effect of treating the maize population volume without spike organs as the AGB is more accurate than the traditional VI model [54]. However, previous studies did not compare different combinations of three-dimensional features and only performed comparisons with a single VI model. Therefore, this study explored whether this 3DCM could be applied to winter wheat and compared its performance with traditional VI model and traditional multi-feature combination model.

Compared with the traditional VI model, the 3DCM performed better in estimating the AGB of winter wheat during the jointing stage (Figure 5), which was similar to the results of Shu et al. [54]. However, the study of Shu et al. [54] did not compare the accuracy

of the 3DCM with that of the traditional multi-feature combination model. Therefore, this study compared the accuracy of the 3DCM with the traditional multi-feature combination model (Figure 6). The results showed that the accuracy of the 3DCM was higher than that of the traditional multi-feature combination model at the jointing stage. However, the accuracy for the other growth stages was similar to that of the traditional multi-feature combination model. This indicates that although the volume-based 3DCM has some potential for estimating the AGB of winter wheat, it has some limitations in estimating the AGB of winter wheat during the whole reproductive stage. This may be due to the emergence of a spike organ. Many studies have shown that photosynthetic products are usually transferred to the reproductive organs of the crop (e.g., wheat spikes) at late stages of growth [62,87,88]. Therefore, considering only stem and leaf organs may lead to an underestimation of the winter wheat AGB at the reproductive growth stage.

Therefore, this study proposed the n3DCM to improve the model's universality in multiple growth stages. The n3DCM mainly considered the impact of spike organ (the SN) on AGB estimation. This study compared the n3DCM (Figure 7A,B) with the 3DCM (Figure 6C,D). The accuracy of the n3DCM was significantly improved after the jointing stage, indicating that adding the SN could effectively improve the model accuracy to estimate the winter wheat AGB during the whole growth stage. This study also compared the n3DCM with the traditional multi-feature combination model of PH, FVC, and SN (Figure 7), and the results showed that the effect of the n3DCM was better than that of the traditional multi-feature combination model. These results indicate that the 3DCM of fused SN can effectively consider the influence of the spike organ on the AGB estimation of winter wheat.

In order to further explore the performance of the n3DCM, the PH and FVC extracted from the two UAVs were combined to estimate the winter wheat AGB (Figure 8). The overall estimated accuracy was above 0.7, but the R^2 of the Fun [(PH_{MS} × FVC_{RGB}), SN] model at the jointing stage was 0.58, which was lower than the overall level. In addition, the n3DCM based on multi-source data fusion did not significantly improve accuracy in estimating the winter wheat AGB. RGB and MS UAVs are equipped with optical sensors, with differences only in band and resolution. Because the flight height in the current study was 30 m, the extracted PH and FVC features were less affected by spectral bands and spatial resolution. Therefore, in this study, the feature combination of multi-source UAVs did not significantly impact the n3DCM.

4.4. Limitations and Prospects

Although the n3DCM was more effective than the traditional method in estimating the AGB of winter wheat, it has some limitations. For example, the measured number of spikes was used to represent the weight of spike organ. Crop spike detection using image recognition techniques is already available [89,90], and these techniques can be used for spike counting. This study selected the "ExG-ExR" threshold method to extract the vegetation elements of winter wheat due to the convenience of operation. However, the "ExG-ExR" method, which is an effective indicator to distinguish green vegetation pixels from the original image, is strictly limited to green objects and is not sensitive to non-green objects [91]. Previous studies have shown that supervised classification methods (e.g., SVM and RF) can provide higher classification accuracy and lower uncertainty [92,93]. Therefore, supervised classification methods can be considered instead of the "ExG-ExR" threshold method in future work.

Although the n3DCM obtained good performance in estimating winter wheat AGB, the results of this study were based on four growth stages in one year and a single location consisting of a combination of varieties and N rates. Therefore, further exploration of the potential of n3DCM must be carried out by utilizing additional locations, winter wheat varieties, nitrogen rates, and growth stages to verify the portability of the model. In addition, investigating how to apply the n3DCM to satellite scales for global applications is also worthy of continued research [23]. This study evaluated the performance of the

winter wheat population volume in estimating the winter wheat AGB but neglected the effect of planting density on estimating the winter wheat AGB [94]. Future work should also consider the effect of crop planting density on the estimation of the winter wheat AGB using the n3DCM.

5. Conclusions

This study investigated the potential of the 3DCM for estimating the winter wheat AGB based on UAV data. The performances of three models on the winter wheat AGB were compared at different growth stages and under different UAVs. Compared with the traditional VI model, the 3DCM performed better in the jointing stage, but its accuracy decreased significantly after the jointing stage. Compared with the traditional multi-feature combination model, the 3DCM only performed better in the jointing stage. In order to enhance the stability of the 3DCM in estimating the winter wheat AGB at different growth stages, an n3DCM was proposed. Compared with the previous three models, the accuracy of the n3DCM was significantly improved after the jointing stage. The R^2 and nRMSE values of the n3DCM were all higher than 0.73 and less than 0.23, respectively, at different growth stages of winter wheat. These results indicate that the n3DCM has great potential in estimating the AGB of winter wheat. The n3DCM provides a new way to estimate the AGB of winter wheat and has excellent potential in the accurate estimation of growth parameters for other crops.

Author Contributions: X.L., W.W., J.L. and Y.Z. were responsible for the conception and design of this research study. Y.Z. analyzed the results of the research and wrote the manuscript. J.L. debugged the algorithm code. X.L., W.W., W.L., J.L., X.T., H.Z. and X.S. repeatedly revised the manuscript. Y.Z., X.T. and X.S. were responsible for data collection and processing in this research. All authors have read and agreed to the published version of the manuscript.

Funding: This project was supported by the National Key Research and Development Program of China (no. 2022YFD2300221), National Key Field Innovation Team Program of China (no. 2021-11), scientific research projects in higher education institutions of Anhui Province (nos. 2022AH051623, 2022AH051029, KJ2021A0891, and KJ2021A0860), Science and Technology Project Program of Fengyang Country, Anhui Province, China (no. NY2022-01), and College Students' Innovation and Entrepreneurship Training Project (no. 202210879043).

Data Availability Statement: Data will be made available upon request.

Acknowledgments: We are very grateful to Xiaofang Chen, Jun Li, Xueqing Zhu, Qingyang Liu, and Weiqiang Wang for their assistance in data collection.

Conflicts of Interest: The authors declare no conflict of interest.

References

1. Fan, L.; Yang, J.; Sun, X.; Zhao, F.; Liang, S.; Duan, D.; Chen, H.; Xia, L.; Sun, J.; Yang, P. The effects of Landsat image acquisition date on winter wheat classification in the North China Plain. *ISPRS-J. Photogramm. Remote Sens.* **2022**, *187*, 1–13. [\[CrossRef\]](#)
2. Shiferaw, B.; Smale, M.; Braun, H.; Duveiller, E.; Reynolds, M.; Muricho, G. Crops that feed the world 10. Past successes and future challenges to the role played by wheat in global food security. *Food Secur.* **2013**, *5*, 291–317. [\[CrossRef\]](#)
3. Fischer, R.A.; Byerlee, D.; Edmeades, G. *Crop Yields and Global Food Security*; Aciar: Canberra, ACT, Australia, 2014; pp. 8–11.
4. Curtis, T.; Halford, N.G. Food security: The challenge of increasing wheat yield and the importance of not compromising food safety. *Ann. Appl. Biol.* **2014**, *164*, 354–372. [\[CrossRef\]](#) [\[PubMed\]](#)
5. Liu, J.; Pattey, E.; Miller, J.R.; McNairn, H.; Smith, A.; Hu, B. Estimating crop stresses, aboveground dry biomass and yield of corn using multi-temporal optical data combined with a radiation use efficiency model. *Remote Sens. Environ.* **2010**, *114*, 1167–1177. [\[CrossRef\]](#)
6. Ritchie, J.T.; Singh, U.; Godwin, D.C.; Bowen, W.T. Cereal growth, development and yield. In *Understanding Options for Agricultural Production*; Springer: Dordrecht, The Netherlands, 1998; pp. 79–98.
7. Lu, N.; Zhou, J.; Han, Z.; Li, D.; Cao, Q.; Yao, X.; Tian, Y.; Zhu, Y.; Cao, W.; Cheng, T. Improved estimation of aboveground biomass in wheat from RGB imagery and point cloud data acquired with a low-cost unmanned aerial vehicle system. *Plant Methods* **2019**, *15*, 17. [\[CrossRef\]](#)
8. Feng, H.; Tao, H.; Fan, Y.; Liu, Y.; Li, Z.; Yang, G.; Zhao, C. Comparison of winter wheat yield estimation based on near-surface hyperspectral and UAV hyperspectral remote sensing data. *Remote Sens.* **2022**, *14*, 4158. [\[CrossRef\]](#)

9. Huang, H.; Huang, J.; Li, X.; Zhuo, W.; Wu, Y.; Niu, Q.; Su, W.; Yuan, W. A dataset of winter wheat aboveground biomass in China during 2007–2015 based on data assimilation. *Sci. Data* **2022**, *9*, 200. [[CrossRef](#)]
10. Fu, Y.; Yang, G.; Song, X.; Li, Z.; Xu, X.; Feng, H.; Zhao, C. Improved estimation of winter wheat aboveground biomass using multiscale textures extracted from UAV-based digital images and hyperspectral feature analysis. *Remote Sens.* **2021**, *13*, 581. [[CrossRef](#)]
11. Navarro, J.A.; Algeet, N.; Fernández-Landa, A.; Esteban, J.; Rodríguez-Noriega, P.; Guillén-Climent, M.L. Integration of UAV, Sentinel-1, and Sentinel-2 data for mangrove plantation aboveground biomass monitoring in Senegal. *Remote Sens.* **2019**, *11*, 77. [[CrossRef](#)]
12. Poley, L.G.; McDermid, J.G. A systematic review of the factors influencing the estimation of vegetation aboveground biomass using unmanned aerial systems. *Remote Sens.* **2020**, *12*, 1052. [[CrossRef](#)]
13. Jin, X.; Kumar, L.; Li, Z.; Feng, H.; Xu, X.; Yang, G.; Wang, J. A review of data assimilation of remote sensing and crop models. *Eur. J. Agron.* **2018**, *92*, 141–152. [[CrossRef](#)]
14. Cavender-Bares, J.; Gamon, J.A.; Townsend, P.A. The use of remote sensing to enhance biodiversity monitoring and detection: A critical challenge for the twenty-first century. In *Remote Sensing of Plant Biodiversity*; Springer: Berlin/Heidelberg, Germany, 2020; pp. 1–12.
15. Knipling, E.B. Physical and physiological basis for the reflectance of visible and near-infrared radiation from vegetation. *Remote Sens. Environ.* **1970**, *1*, 155–159. [[CrossRef](#)]
16. Zhou, K.; Cheng, T.; Zhu, Y.; Cao, W.; Ustin, S.L.; Zheng, H.; Yao, X.; Tian, Y. Assessing the impact of spatial resolution on the estimation of leaf nitrogen concentration over the full season of paddy rice using near-surface imaging spectroscopy data. *Front. Plant Sci.* **2018**, *9*, 964. [[CrossRef](#)]
17. Yue, J.; Feng, H.; Yang, G.; Li, Z. A comparison of regression techniques for estimation of above-ground winter wheat biomass using near-surface spectroscopy. *Remote Sens.* **2018**, *10*, 66. [[CrossRef](#)]
18. Liu, J.; Zhu, Y.; Tao, X.; Chen, X.; Li, X. Rapid prediction of winter wheat yield and nitrogen use efficiency using consumer-grade unmanned aerial vehicles multispectral imagery. *Front. Plant Sci.* **2022**, *13*, 1032170. [[CrossRef](#)]
19. Wang, W.; Zheng, H.; Wu, Y.; Yao, X.; Zhu, Y.; Cao, W.; Cheng, T. An assessment of background removal approaches for improved estimation of rice leaf nitrogen concentration with unmanned aerial vehicle multispectral imagery at various observation times. *Field Crops Res.* **2022**, *283*, 108543. [[CrossRef](#)]
20. Zheng, J.; Fu, H.; Li, W.; Wu, W.; Yu, L.; Yuan, S.; Tao, W.Y.W.; Pang, T.K.; Kanniah, K.D. Growing status observation for oil palm trees using Unmanned Aerial Vehicle (UAV) images. *ISPRS-J. Photogramm. Remote Sens.* **2021**, *173*, 95–121. [[CrossRef](#)]
21. Zhou, W.; Liu, Y.; Ata-Ul-Karim, S.T.; Ge, Q.; Li, X.; Xiao, J. Integrating climate and satellite remote sensing data for predicting county-level wheat yield in China using machine learning methods. *Int. J. Appl. Earth Obs. Geoinf.* **2022**, *111*, 102861. [[CrossRef](#)]
22. Cai, Y.; Guan, K.; Lobell, D.; Potgieter, A.B.; Wang, S.; Peng, J.; Xu, T.; Asseng, S.; Zhang, Y.; You, L. Integrating satellite and climate data to predict wheat yield in Australia using machine learning approaches. *Agric. For. Meteorol.* **2019**, *274*, 144–159. [[CrossRef](#)]
23. Zheng, J.; Yuan, S.; Wu, W.; Li, W.; Yu, L.; Fu, H.; Coomes, D. Surveying coconut trees using high-resolution satellite imagery in remote atolls of the Pacific Ocean. *Remote Sens. Environ.* **2023**, *287*, 113485. [[CrossRef](#)]
24. Tian, Y.; Gu, K.; Chu, X.; Yao, X.; Cao, W.; Zhu, Y. Comparison of different hyperspectral vegetation indices for canopy leaf nitrogen concentration estimation in rice. *Plant Soil* **2014**, *376*, 193–209. [[CrossRef](#)]
25. Omer, G.; Mutanga, O.; Abdel-Rahman, E.M.; Peerbhay, K.; Adam, E. Mapping leaf nitrogen and carbon concentrations of intact and fragmented indigenous forest ecosystems using empirical modeling techniques and WorldView-2 data. *ISPRS-J. Photogramm. Remote Sens.* **2017**, *131*, 26–39. [[CrossRef](#)]
26. Xie, C.; Yang, C. A review on plant high-throughput phenotyping traits using UAV-based sensors. *Comput. Electron. Agric.* **2020**, *178*, 105731. [[CrossRef](#)]
27. Sankaran, S.; Khot, L.R.; Espinoza, C.Z.; Jarolmasjed, S.; Sathuvalli, V.R.; Vandemark, G.J.; Miklas, P.N.; Carter, A.H.; Pumphrey, M.O.; Knowles, N.R. Low-altitude, high-resolution aerial imaging systems for row and field crop phenotyping: A review. *Eur. J. Agron.* **2015**, *70*, 112–123. [[CrossRef](#)]
28. Rouse, J.W.; Haas, R.H.; Schell, J.A.; Deering, D.W. Monitoring vegetation systems in the Great Plains with ERTS. *Nasa Spec. Publ.* **1974**, *351*, 309.
29. Mao, W.; Wang, Y.; Wang, Y. Real-time detection of between-row weeds using machine vision. In Proceedings of the 2003 ASAE Annual Meeting: American Society of Agricultural and Biological Engineers, Las Vegas, NV, USA, 27–30 July 2003; p. 1.
30. Niu, Y.; Zhang, L.; Zhang, H.; Han, W.; Peng, X. Estimating above-ground biomass of maize using features derived from UAV-based RGB imagery. *Remote Sens.* **2019**, *11*, 1261. [[CrossRef](#)]
31. Wang, F.; Yang, M.; Ma, L.; Zhang, T.; Qin, W.; Li, W.; Zhang, Y.; Sun, Z.; Wang, Z.; Li, F. Estimation of above-ground biomass of winter wheat based on consumer-grade multi-spectral UAV. *Remote Sens.* **2022**, *14*, 1251. [[CrossRef](#)]
32. Wan, L.; Cen, H.; Zhu, J.; Zhang, J.; Zhu, Y.; Sun, D.; Du, X.; Zhai, L.; Weng, H.; Li, Y. Grain yield prediction of rice using multi-temporal UAV-based RGB and multispectral images and model transfer—A case study of small farmlands in the South of China. *Agric. For. Meteorol.* **2020**, *291*, 108096. [[CrossRef](#)]
33. Han, L.; Yang, G.; Dai, H.; Xu, B.; Yang, H.; Feng, H.; Li, Z.; Yang, X. Modeling maize above-ground biomass based on machine learning approaches using UAV remote-sensing data. *Plant Methods* **2019**, *15*, 10. [[CrossRef](#)]

34. Swoish, M.; Leme Filho, J.F.D.C.; Reiter, M.S.; Campbell, J.B.; Thomason, W.E. Comparing satellites and vegetation indices for cover crop biomass estimation. *Comput. Electron. Agric.* **2022**, *196*, 106900. [[CrossRef](#)]
35. Mutanga, O.; Masenyama, A.; Sibanda, M. Spectral saturation in the remote sensing of high-density vegetation traits: A systematic review of progress, challenges, and prospects. *ISPRS-J. Photogramm. Remote Sens.* **2023**, *198*, 297–309. [[CrossRef](#)]
36. Li, Z.; Taylor, J.; Yang, H.; Casa, R.; Jin, X.; Li, Z.; Song, X.; Yang, G. A hierarchical interannual wheat yield and grain protein prediction model using spectral vegetative indices and meteorological data. *Field Crops Res.* **2020**, *248*, 107711. [[CrossRef](#)]
37. Jiang, Z.; Huete, A.R.; Didan, K.; Miura, T. Development of a two-band enhanced vegetation index without a blue band. *Remote Sens. Environ.* **2008**, *112*, 3833–3845. [[CrossRef](#)]
38. Yue, J.; Yang, G.; Tian, Q.; Feng, H.; Xu, K.; Zhou, C. Estimate of winter-wheat above-ground biomass based on UAV ultrahigh-ground-resolution image textures and vegetation indices. *ISPRS-J. Photogramm. Remote Sens.* **2019**, *150*, 226–244. [[CrossRef](#)]
39. Mutanga, O.; Skidmore, A.K. Narrow band vegetation indices overcome the saturation problem in biomass estimation. *Int. J. Remote Sens.* **2004**, *25*, 3999–4014. [[CrossRef](#)]
40. Zaman-Allah, M.; Vergara, O.; Araus, J.L.; Tarekegne, A.; Magorokosho, C.; Zarco-Tejada, P.J.; Hornero, A.; Albà, A.H.; Das, B.; Craufurd, P. Unmanned aerial platform-based multi-spectral imaging for field phenotyping of maize. *Plant Methods* **2015**, *11*, 35. [[CrossRef](#)]
41. Haboudane, D.; Tremblay, N.; Miller, J.R.; Vigneault, P. Remote estimation of crop chlorophyll content using spectral indices derived from hyperspectral data. *IEEE Trans. Geosci. Remote Sens.* **2008**, *46*, 423–437. [[CrossRef](#)]
42. Cui, B.; Zhao, Q.; Huang, W.; Song, X.; Ye, H.; Zhou, X. A new integrated vegetation index for the estimation of winter wheat leaf chlorophyll content. *Remote Sens.* **2019**, *11*, 974. [[CrossRef](#)]
43. Li, F.; Miao, Y.; Feng, G.; Yuan, F.; Yue, S.; Gao, X.; Liu, Y.; Liu, B.; Ustin, S.L.; Chen, X. Improving estimation of summer maize nitrogen status with red edge-based spectral vegetation indices. *Field Crops Res.* **2014**, *157*, 111–123. [[CrossRef](#)]
44. Gnyp, M.L.; Bareth, G.; Li, F.; Lenz-Wiedemann, V.I.; Koppe, W.; Miao, Y.; Hennig, S.D.; Jia, L.; Laudien, R.; Chen, X. Development and implementation of a multiscale biomass model using hyperspectral vegetation indices for winter wheat in the North China Plain. *Int. J. Appl. Earth Obs. Geoinf.* **2014**, *33*, 232–242. [[CrossRef](#)]
45. Liu, Y.; Liu, S.; Li, J.; Guo, X.; Wang, S.; Lu, J. Estimating biomass of winter oilseed rape using vegetation indices and texture metrics derived from UAV multispectral images. *Comput. Electron. Agric.* **2019**, *166*, 105026. [[CrossRef](#)]
46. Tilly, N.; Aasen, H.; Bareth, G. Fusion of plant height and vegetation indices for the estimation of barley biomass. *Remote Sens.* **2015**, *7*, 11449–11480. [[CrossRef](#)]
47. Yue, J.; Yang, G.; Li, C.; Li, Z.; Wang, Y.; Feng, H.; Xu, B. Estimation of winter wheat above-ground biomass using unmanned aerial vehicle-based snapshot hyperspectral sensor and crop height improved models. *Remote Sens.* **2017**, *9*, 708. [[CrossRef](#)]
48. Bendig, J.; Bolten, A.; Bennertz, S.; Broscheit, J.; Eichfuss, S.; Bareth, G. Estimating biomass of barley using crop surface models (CSMs) derived from UAV-based RGB imaging. *Remote Sens.* **2014**, *6*, 10395–10412. [[CrossRef](#)]
49. Martínez-Guanter, J.; Egea, G.; Pérez-Ruiz, M.; Apolo-Apolo, O.E. Estimation of the leaf area index in maize based on UAV imagery using deep learning techniques. In *Precision Agriculture'19*; Wageningen Academic Publishers: Wageningen, The Netherlands, 2019; p. 1304.
50. Luo, S.; Jiang, X.; He, Y.; Li, J.; Jiao, W.; Zhang, S.; Xu, F.; Han, Z.; Sun, J.; Yang, J. Multi-dimensional variables and feature parameter selection for aboveground biomass estimation of potato based on UAV multispectral imagery. *Front. Plant Sci.* **2022**, *13*, 2673. [[CrossRef](#)]
51. Sadeghi, Y.; St-Onge, B.; Leblon, B.; Prieur, J.; Simard, M. Mapping boreal forest biomass from a SRTM and TanDEM-X based on canopy height model and Landsat spectral indices. *Int. J. Appl. Earth Obs. Geoinf.* **2018**, *68*, 202–213. [[CrossRef](#)]
52. Fei, S.; Hassan, M.A.; Xiao, Y.; Su, X.; Chen, Z.; Cheng, Q.; Duan, F.; Chen, R.; Ma, Y. UAV-based multi-sensor data fusion and machine learning algorithm for yield prediction in wheat. *Precis. Agric.* **2023**, *24*, 187–212. [[CrossRef](#)]
53. Bendig, J.; Yu, K.; Aasen, H.; Bolten, A.; Bennertz, S.; Broscheit, J.; Gnyp, M.L.; Bareth, G. Combining UAV-based plant height from crop surface models, visible, and near infrared vegetation indices for biomass monitoring in barley. *Int. J. Appl. Earth Obs. Geoinf.* **2015**, *39*, 79–87. [[CrossRef](#)]
54. Meiyan, S.; Mengyuan, S.; Qizhou, D.; Xiaohong, Y.; Baoguo, L.; Yuntao, M. Estimating the maize above-ground biomass by constructing the tridimensional concept model based on UAV-based digital and multi-spectral images. *Field Crops Res.* **2022**, *282*, 108491. [[CrossRef](#)]
55. Yuan, Q.; Shen, H.; Li, T.; Li, Z.; Li, S.; Jiang, Y.; Xu, H.; Tan, W.; Yang, Q.; Wang, J. Deep learning in environmental remote sensing: Achievements and challenges. *Remote Sens. Environ.* **2020**, *241*, 111716. [[CrossRef](#)]
56. Weiss, M.; Jacob, F.; Duveiller, G. Remote sensing for agricultural applications: A meta-review. *Remote Sens. Environ.* **2020**, *236*, 111402. [[CrossRef](#)]
57. Liakos, K.G.; Busato, P.; Moshou, D.; Pearson, S.; Bochtis, D. Machine learning in agriculture: A review. *Sensors* **2018**, *18*, 2674. [[CrossRef](#)]
58. Lu, D. The potential and challenge of remote sensing-based biomass estimation. *Int. J. Remote Sens.* **2006**, *27*, 1297–1328. [[CrossRef](#)]
59. Li, B.; Xu, X.; Zhang, L.; Han, J.; Bian, C.; Li, G.; Liu, J.; Jin, L. Above-ground biomass estimation and yield prediction in potato by using UAV-based RGB and hyperspectral imaging. *ISPRS-J. Photogramm. Remote Sens.* **2020**, *162*, 161–172. [[CrossRef](#)]
60. Zhu, W.; Sun, Z.; Yang, T.; Li, J.; Peng, J.; Zhu, K.; Li, S.; Gong, H.; Lyu, Y.; Li, B. Estimating leaf chlorophyll content of crops via optimal unmanned aerial vehicle hyperspectral data at multi-scales. *Comput. Electron. Agric.* **2020**, *178*, 105786. [[CrossRef](#)]

61. Li, Q.; Jin, S.; Zang, J.; Wang, X.; Sun, Z.; Li, Z.; Xu, S.; Ma, Q.; Su, Y.; Guo, Q. Deciphering the contributions of spectral and structural data to wheat yield estimation from proximal sensing. *Crop J.* **2022**, *10*, 1334–1345. [[CrossRef](#)]
62. Yue, J.; Yang, H.; Yang, G.; Fu, Y.; Wang, H.; Zhou, C. Estimating vertically growing crop above-ground biomass based on UAV remote sensing. *Comput. Electron. Agric.* **2023**, *205*, 107627. [[CrossRef](#)]
63. Wang, Q.; Che, Y.; Shao, K.; Zhu, J.; Wang, R.; Sui, Y.; Guo, Y.; Li, B.; Meng, L.; Ma, Y. Estimation of sugar content in sugar beet root based on UAV multi-sensor data. *Comput. Electron. Agric.* **2022**, *203*, 107433. [[CrossRef](#)]
64. Fu, Z.; Jiang, J.; Gao, Y.; Krienke, B.; Wang, M.; Zhong, K.; Cao, Q.; Tian, Y.; Zhu, Y.; Cao, W. Wheat growth monitoring and yield estimation based on multi-rotor unmanned aerial vehicle. *Remote Sens.* **2020**, *12*, 508. [[CrossRef](#)]
65. Berni, J.; Zarco-Tejada, P.J.; Suarez, L.; González-Dugo, V.; Fereres, E. Remote sensing of vegetation from UAV platforms using lightweight multispectral and thermal imaging sensors. *Int. Arch. Photogramm. Remote Sens. Spatial Inform. Sci.* **2009**, *38*, 6.
66. Zhang, J.; Qiu, X.; Wu, Y.; Zhu, Y.; Cao, Q.; Liu, X.; Cao, W. Combining texture, color, and vegetation indices from fixed-wing UAS imagery to estimate wheat growth parameters using multivariate regression methods. *Comput. Electron. Agric.* **2021**, *185*, 106138. [[CrossRef](#)]
67. Lowe, D.G. Distinctive image features from scale-invariant keypoints. *Int. J. Comput. Vis.* **2004**, *60*, 91–110. [[CrossRef](#)]
68. Li, L.; Mu, X.; Jiang, H.; Chianucci, F.; Hu, R.; Song, W.; Qi, J.; Liu, S.; Zhou, J.; Chen, L.; et al. Review of ground and aerial methods for vegetation cover fraction (fCover) and related quantities estimation: Definitions, advances, challenges, and future perspectives. *ISPRS-J. Photogramm. Remote Sens.* **2023**, *199*, 133–156. [[CrossRef](#)]
69. Meyer, G.E.; Neto, J.C. Verification of color vegetation indices for automated crop imaging applications. *Comput. Electron. Agric.* **2008**, *63*, 282–293. [[CrossRef](#)]
70. Breiman, L. Random forests. *Mach. Learn.* **2001**, *45*, 5–32. [[CrossRef](#)]
71. Belgiu, M.; Drăguț, L. Random forest in remote sensing: A review of applications and future directions. *ISPRS-J. Photogramm. Remote Sens.* **2016**, *114*, 24–31. [[CrossRef](#)]
72. Zhou, X.; Zhu, X.; Dong, Z.; Guo, W. Estimation of biomass in wheat using random forest regression algorithm and remote sensing data. *Crop J.* **2016**, *4*, 212–219.
73. Hastie, T.; Tibshirani, R.; Friedman, J.; Hastie, T.; Tibshirani, R.; Friedman, J. Unsupervised learning. In *The Elements of Statistical Learning: Data Mining, Inference, and Prediction*; Springer: Berlin/Heidelberg, Germany, 2009; pp. 485–585.
74. Hutengs, C.; Vohland, M. Downscaling land surface temperatures at regional scales with random forest regression. *Remote Sens. Environ.* **2016**, *178*, 127–141. [[CrossRef](#)]
75. Zhang, Y.; Xia, C.; Zhang, X.; Cheng, X.; Feng, G.; Wang, Y.; Gao, Q. Estimating the maize biomass by crop height and narrowband vegetation indices derived from UAV-based hyperspectral images. *Ecol. Indic.* **2021**, *129*, 107985. [[CrossRef](#)]
76. Madec, S.; Baret, F.; de Solan, B.; Thomas, S.; Dutartre, D.; Jezequel, S.; Hemmerlé, M.; Colombeau, G.; Comar, A. High-Throughput Phenotyping of Plant Height: Comparing Unmanned Aerial Vehicles and Ground LiDAR Estimates. *Front. Plant Sci.* **2017**, *8*, 2002. [[CrossRef](#)]
77. Li, W.; Niu, Z.; Chen, H.; Li, D.; Wu, M.; Zhao, W. Remote estimation of canopy height and aboveground biomass of maize using high-resolution stereo images from a low-cost unmanned aerial vehicle system. *Ecol. Indic.* **2016**, *67*, 637–648. [[CrossRef](#)]
78. Huete, A.R.; Jackson, R.D.; Post, D.F. Spectral response of a plant canopy with different soil backgrounds. *Remote Sens. Environ.* **1985**, *17*, 37–53. [[CrossRef](#)]
79. Klemas, V.; Smart, R. The influence of soil salinity, growth form, and leaf moisture on-the spectral radiance of. *Photogramm. Eng. Remote Sens.* **1983**, *49*, 77–83.
80. Zhou, X.; Yang, M.; Chen, X.; Ma, L.; Yin, C.; Qin, S.; Wang, L.; Lv, X.; Zhang, Z. Estimation of Cotton Nitrogen Content Based on Multi-Angle Hyperspectral Data and Machine Learning Models. *Remote Sens.* **2023**, *15*, 955. [[CrossRef](#)]
81. He, L.; Liu, M.; Guo, Y.; Wei, Y.; Zhang, H.; Song, X.; Feng, W.; Guo, T. Angular effect of algorithms for monitoring leaf nitrogen concentration of wheat using multi-angle remote sensing data. *Comput. Electron. Agric.* **2022**, *195*, 106815. [[CrossRef](#)]
82. Li, D.; Chen, J.M.; Zhang, X.; Yan, Y.; Zhu, J.; Zheng, H.; Zhou, K.; Yao, X.; Tian, Y.; Zhu, Y. Improved estimation of leaf chlorophyll content of row crops from canopy reflectance spectra through minimizing canopy structural effects and optimizing off-noon observation time. *Remote Sens. Environ.* **2020**, *248*, 111985. [[CrossRef](#)]
83. Thomas, S.; Kuska, M.T.; Bohnenkamp, D.; Brugger, A.; Alisaac, E.; Wahabzada, M.; Behmann, J.; Mahlein, A. Benefits of hyperspectral imaging for plant disease detection and plant protection: A technical perspective. *J. Plant Dis. Prot.* **2018**, *125*, 5–20. [[CrossRef](#)]
84. Ehlert, D.; Horn, H.; Adamek, R. Measuring crop biomass density by laser triangulation. *Comput. Electron. Agric.* **2008**, *61*, 117–125. [[CrossRef](#)]
85. Wan, L.; Zhu, J.; Du, X.; Zhang, J.; Han, X.; Zhou, W.; Li, X.; Liu, J.; Liang, F.; He, Y. A model for phenotyping crop fractional vegetation cover using imagery from unmanned aerial vehicles. *J. Exp. Bot.* **2021**, *72*, 4691–4707. [[CrossRef](#)]
86. Li, Z.; Zhao, Y.; Taylor, J.; Gaulton, R.; Jin, X.; Song, X.; Li, Z.; Meng, Y.; Chen, P.; Feng, H. Comparison and transferability of thermal, temporal and phenological-based in-season predictions of above-ground biomass in wheat crops from proximal crop reflectance data. *Remote Sens. Environ.* **2022**, *273*, 112967. [[CrossRef](#)]
87. Makanza, R.; Zaman-Allah, M.; Cairns, J.E.; Magorokosho, C.; Tarekegne, A.; Olsen, M.; Prasanna, B.M. High-throughput phenotyping of canopy cover and senescence in maize field trials using aerial digital canopy imaging. *Remote Sens.* **2018**, *10*, 330. [[CrossRef](#)] [[PubMed](#)]

88. Wang, Y.; Zhang, K.; Tang, C.; Cao, Q.; Tian, Y.; Zhu, Y.; Cao, W.; Liu, X. Estimation of rice growth parameters based on linear mixed-effect model using multispectral images from fixed-wing unmanned aerial vehicles. *Remote Sens.* **2019**, *11*, 1371. [[CrossRef](#)]
89. Sun, J.; Yang, K.; Chen, C.; Shen, J.; Yang, Y.; Wu, X.; Norton, T. Wheat head counting in the wild by an augmented feature pyramid networks-based convolutional neural network. *Comput. Electron. Agric.* **2022**, *193*, 106705. [[CrossRef](#)]
90. Zaji, A.; Liu, Z.; Xiao, G.; Bhowmik, P.; Sangha, J.S.; Ruan, Y. AutoOLA: Automatic object level augmentation for wheat spikes counting. *Comput. Electron. Agric.* **2023**, *205*, 107623. [[CrossRef](#)]
91. Tian, K.; Li, J.; Zeng, J.; Evans, A.; Zhang, L. Segmentation of tomato leaf images based on adaptive clustering number of K-means algorithm. *Comput. Electron. Agric.* **2019**, *165*, 104962. [[CrossRef](#)]
92. Buciu, I.; Kotropoulos, C.; Pitas, I. Demonstrating the stability of support vector machines for classification. *Signal Process.* **2006**, *86*, 2364–2380. [[CrossRef](#)]
93. Rodriguez-Galiano, V.F.; Chica-Olmo, M.; Abarca-Hernandez, F.; Atkinson, P.M.; Jeganathan, C. Random Forest classification of Mediterranean land cover using multi-seasonal imagery and multi-seasonal texture. *Remote Sens. Environ.* **2012**, *121*, 93–107. [[CrossRef](#)]
94. Bates, J.S.; Montzka, C.; Schmidt, M.; Jonard, F. Estimating Canopy Density Parameters Time-Series for Winter Wheat Using UAS Mounted LiDAR. *Remote Sens.* **2021**, *13*, 710. [[CrossRef](#)]

Disclaimer/Publisher’s Note: The statements, opinions and data contained in all publications are solely those of the individual author(s) and contributor(s) and not of MDPI and/or the editor(s). MDPI and/or the editor(s) disclaim responsibility for any injury to people or property resulting from any ideas, methods, instructions or products referred to in the content.